A Finite Element Dual Porosity Approach to Model Deformation-Induced Fluid Flow in Cortical Bone

Pere Fornells, José Manuel García-Aznar, and Manuel Doblaré

Group of Structural Mechanics and Material Modeling, Mechanical Engineering Department, Aragon Institute of Engineering Research (I3A), University of Zaragoza, María de Luna, 3, E-50018 Zaragoza, Spain

Abstract—Fluid flow through the osteocyte canaliculi network is widely believed to be a main factor that controls bone adaptation. The difficulty of in vivo measurement of this flow within cortical bone makes computational models an appealing alternative to estimate it. We present in this paper a finite element dual porosity macroscopic model that can contribute to evaluate the interstitial fluid flow induced by mechanical loads in large pieces of bone. This computational model allows us to predict the macroscopic fluid flow at both vascular and canalicular porosities in a whole loaded bone. Our results confirm that the general trend in the fluid flow field predicted is similar to the one obtained with previous microscopic models, and that in a whole bone model it is able to estimate the zones with higher bone remodeling.

Keywords—Cortical bone, Poroelasticity, Dual porosity, Interstitial fluid flow, Finite element analysis, Bone remodeling.

INTRODUCTION

Bone is a highly structured composite material with a hierarchical network of flow channels with different characteristic dimensions.[8] In fact, cortical bone has three main levels of porosity with different dimensions and characteristics:[8] vascular porosity (PV) is associated with blood irrigation and has a radius in the order of 20 μm; lacuno-canalicular porosity (PLC) is associated with the lacunae where the osteocytes are located and with the canaliculi that connect them (order of 0.1 μm); and collagen-apatite porosity (PCA) associated with the spaces between collagen and mineral (order of 10 nm radius). All of these porosities are filled with bone fluid, but in PCA the fluid flow is negligible.[8]

Bone has also the well-known property of adapting its structure to the mechanical environment, tending to a high strength structure with minimum material.[31] This biological process of bone adaptation is well-established, but the specific mechanical stimulus that controls it is not completely understood yet.[9] Current evidences suggest that osteocytes are the mechanosensory cells in bone, and that a possible stimulus is the shear stress induced by canalicular fluid flow.[4,9] Although the increase of the transport capacity induced by fluid flow is also considered an important effect in the mechanosensory bone system. Unfortunately, it is very difficult to directly measure fluid flow velocities and shear stresses within the lacuno-canalicular system.[5] Therefore, computational models have been used to estimate these quantities.[3,7,14,19,23,26,30] Most of these works study fluid flow in bone from a microscopic point of view, simulating a small part taking into account the microstructural details of the osteonal canals. They use poroelasticity to compute the fluid flow in the lacuno-canalicular spaces. Other computational models have determined the load-induced fluid flow at the macroscopic level, but only considering lacuno-canalicular porosity.[26] However, as far as the authors know, there is no model able to simulate a whole bone in order to predict fluid movement through the different bone porosities at a macroscopic level.

Given that hierarchical network of canals, the extension of Biot's concepts of poroelasticity[6] to a dual porosity approach can be very appropriate for cortical bone. The theory of dual porosity, developed in the 70s by Duguid[10,11,12] and Aifantis[1,2] to simulate the flow through fissured porous media, is here used to predict the movement of fluid within cortical bone at two levels of porosity (PV and PLC). Two different models have been developed to test the potential of the dual porosity applied to bone: a 2D model of a small sample of cortical bone, reproducing the simulation of Starkebaum *et al.*[25] and a 3D rat tibia model

Address correspondence to José Manuel García-Aznar, Group of Structural Mechanics and Material Modeling, Mechanical Engineering Department, Aragon Institute of Engineering Research (I3A), University of Zaragoza, María de Luna, 3, E-50018 Zaragoza, Spain. Electronic mail: jmgaraz@unizar.es

reproducing the experiments of Srinivasan *et al.*[24] The ability of this approach to reproduce complex bone behavior and its potential to be used in bone remodeling studies are discussed according to the results obtained with our models.

MATERIALS AND METHODS

Dual Porosity Model

The dual porosity formulation here presented is based on that proposed by Valliappan and Khalili-Naghadeh[15] for the study of rocks as saturated fissured porous media. Its derivation is fully described in Appendix A.

The set of governing equations for the cortical bone tissue is

$$G \frac{\partial^2 u_i}{\partial x_j \partial x_j} + (\lambda + G) \frac{\partial^2 u_j}{\partial x_i \partial x_j} - \alpha_1 \frac{\partial p_1}{\partial x_i} - \alpha_2 \frac{\partial p_2}{\partial x_i} + F_i = 0 \tag{1a}$$

$$\frac{k_1}{\mu} \frac{\partial^2 p_1}{\partial x_i \partial x_i} = a_{11} \frac{\partial p_1}{\partial t} + a_{12} \frac{\partial p_2}{\partial t} + \alpha_1 \frac{\partial^2 u_i}{\partial t \partial x_i} - \frac{\Gamma}{\rho_f} \tag{1b}$$

$$\frac{k_2}{\mu} \frac{\partial^2 p_2}{\partial x_i \partial x_i} = a_{21} \frac{\partial p_1}{\partial t} + a_{22} \frac{\partial p_2}{\partial t} + \alpha_2 \frac{\partial^2 u_i}{\partial t \partial x_i} + \frac{\Gamma}{\rho_f} \tag{1c}$$

$$\frac{\Gamma}{\rho_f} = \gamma(p_1 - p_2) \tag{1d}$$

where λ and G are the so called Lame's constants, α_1 and α_2 are the effective stress coefficients, k_1 and k_2 are the permeabilities of PV and PLC, ρ_f and μ are bone fluid's density and viscosity and γ is the so-called leakage parameter, which modulates the regulating role that bone lining cells perform on bone surfaces controlling the flux of fluid between compartments and the interstitial fluid pressure.[16] The rest of the parameters are defined as

$$a_{11} = \phi_1/K_f + (\alpha_1 - \phi_1)/K_s + \chi/K$$
$$a_{12} = a_{21} = -\chi/K$$
$$a_{22} = \phi_2/K_f + (\alpha_2 - \phi_2)/K_s + \chi/K$$
$$\alpha_1 = K/K_v - K/K_s \tag{2}$$
$$\alpha_2 = 1 - K/K_v$$
$$\chi = \alpha_1 \alpha_2 - \phi_1 \phi_2 \frac{\alpha_1 + \alpha_2}{\phi_1 + \phi_2}$$

being ϕ_1 and ϕ_2 the PV and PLC porosities, K the drained bulk modulus, and K_v and K_s the PV and the bone matrix bulk moduli.

The finite element formulation of the governing equations (1) is obtained by employing the standard Galerkin approach.[28] The resulting system can be expressed as:

$$\boldsymbol{K}\boldsymbol{u}^N - \alpha_1 \boldsymbol{C}\boldsymbol{p}_1^N - \alpha_2 \boldsymbol{C}\boldsymbol{p}_2^N = \boldsymbol{R}$$
$$\alpha_1 \boldsymbol{C}^T \dot{\boldsymbol{u}}^N + (\boldsymbol{H}_1 + \gamma \boldsymbol{M})\boldsymbol{p}_1^N + a_{11}\boldsymbol{M}\dot{\boldsymbol{p}}_1^N + a_{12}\boldsymbol{M}\dot{\boldsymbol{p}}_2^N - \gamma \boldsymbol{M}\boldsymbol{p}_2^N = \boldsymbol{Q}_1$$
$$\alpha_2 \boldsymbol{C}^T \dot{\boldsymbol{u}}^N + (\boldsymbol{H}_2 + \gamma \boldsymbol{M})\boldsymbol{p}_2^N + a_{21}\boldsymbol{M}\dot{\boldsymbol{p}}_1^N + a_{22}\boldsymbol{M}\dot{\boldsymbol{p}}_2^N - \gamma \boldsymbol{M}\boldsymbol{p}_1^N = \boldsymbol{Q}_2 \tag{3}$$

with

$$\boldsymbol{K} = \int_V \boldsymbol{B}_u{}^T \boldsymbol{D} \boldsymbol{B}_u dV \qquad \boldsymbol{C} = \int_V \boldsymbol{B}_u N dV$$
$$\boldsymbol{H}_1 = \int_V \boldsymbol{B}_p{}^T \boldsymbol{K}_1 \boldsymbol{B}_p dV \qquad \boldsymbol{H}_2 = \int_V \boldsymbol{B}_p{}^T \boldsymbol{K}_2 \boldsymbol{B}_p dV$$
$$\boldsymbol{M} = \int_V N^T N dV \qquad \boldsymbol{R} = \int_V N^T \boldsymbol{F} dV + \int_S N^T \boldsymbol{T} dS$$
$$\boldsymbol{Q}_1 = \int_S N^T \boldsymbol{q}_1 dS \qquad \boldsymbol{Q}_2 = \int_S N^T \boldsymbol{q}_2 dS$$

being N the shape functions matrix, $\boldsymbol{B}_u$ and $\boldsymbol{B}_p$ the strain matrices expressed in terms of the derivatives of shape functions employed respectively for displacements and pressures, $\boldsymbol{D}$ the constitutive stress–strain matrix, $\boldsymbol{K}_1$ and $\boldsymbol{K}_2$ the PV and PLC permeability matrices, $\boldsymbol{T}$ the boundary traction vector and $\boldsymbol{q}_\alpha$ the fluid fluxes. Linear interpolation functions were used for displacements and pressures, and a backward Euler time integration scheme was employed to define the velocities in terms of the associated degrees of freedom.

The particularization of this formulation to the case of simple porosity is straightforward, with no more than adding the conditions $a_{21} = a_{12} = a_{22} = \alpha_2 = k_2 = \gamma = 0$, getting the poroelastic **u-p** formulation described for instance in Zienckiewicz and Shiomi.[34]

Numerical Examples

This dual porosity formulation has been implemented in the commercial finite element software Abaqus[20] as a user element routine. Several mechanical load conditions were then simulated in order to check its potential.

Simulation of Bending of a Small Sample of Cortical Bone

We first simulated the experimental work of Starkebaum *et al.*[25] (Fig. 1a), where bending is applied to a small sample of cortical bone (size of a few osteons). A similar sample was also simulated computationally by Wang *et al.*[30] with a microscopical model where Haversian canals were modeled as holes. To take advantage of the symmetry of the problem a rectangle of 1.2×0.1 mm was modeled (Fig. 1b), applying symmetry boundary conditions at the left side of the mesh, and a sinusoidal bending moment (1.5 Hz) at the other side, with the outer fiber strain being 200 $\mu\varepsilon$. The model is composed of 366 nodes and 300 linear, quadrilateral elements. As a first approach, vascular porosity was considered isotropic. Three different values of vascular porosity were simulated: $\phi_1 = 0$ (no PV present), $\phi_1 = 0.03$ and $\phi_1 = 0.07$.
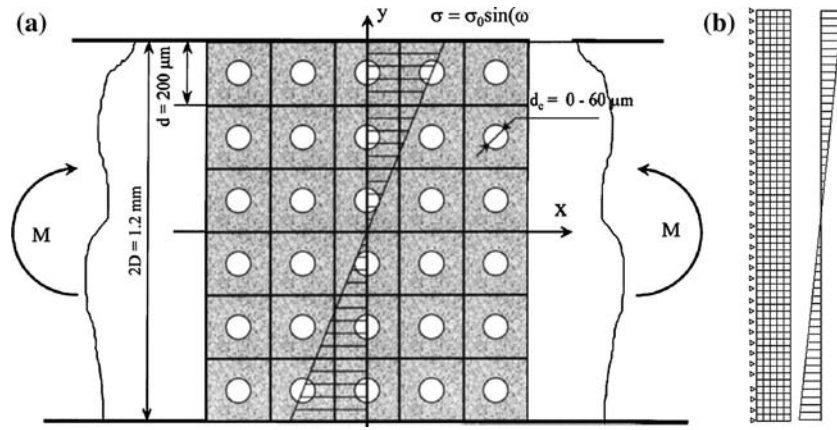
FIGURE 1. (a) Model employed by Wang *et al.* where an idealized section of cortical bone is subjected to bending (taken with permission from Wang *et al.*[30]) (b) Finite Element mesh and boundary conditions. Displacement is defined as $u_x = 5.2 \times 10^{-5}(y/D)\sin \omega t$.

The goal of this simulation was to test if the dual porosity model is able to achieve realistic results in bone tissue, and also analyze the role of the different parameters involved in the results obtained. Following Wang *et al.*,[30] we applied a bending moment so that the outer fiber stress was $tr\sigma = 4$ MPa.

Bone was assumed to have a drained bulk modulus of $K = 12$ Gpa, a solid bulk modulus of $K_s = 16$ Gpa and a drained Poisson's ratio of $v = 0.25$.[33] The fluid bulk modulus was assumed to be the same of salt water ($K_f = 2.3$ Gpa). PV permeability was taken from Cowin[8] as 3×10^{-13} m^2 for $\phi_1 = 0.03$ and 6.36×10^{-13} m^2 for $\phi_1 = 0.07$. PLC was established as $\phi_2 = 0.05$ and its permeability $k_2 = 1.7 \times 10^{-20}$ m^2.[30] We estimated the leakage parameter as $\gamma = 1.7 \times 10^{-9}$ m^2/Ns for $\phi_1 = 0.03$ and $\gamma = 2.7 \times 10^{-9}$ m^2/Ns for $\phi_1 = 0.07$. The vascular compressibility K_v (15 Gpa) was computationally estimated through a microscopic model of a portion of cortical bone characteristic of a Haversian canal. All the parameters used in the simulation have been summarized in Table 1.

With this model, we analyzed the fluid flow induced by cyclic loading under different frequencies. In fact, the influence of the loading frequency in the range from 0.01 to 500 Hz was studied. All pressure results presented correspond to steady state values once they were reached after the sinusoidal load was applied. A sensitivity study was also performed in order to study the influence of the following parameters: leakage

parameter γ from 10^{-12} to 10^{-6} m^2/Ns, vascular permeability from 10^{-14} to 10^{-12} m^2, lacuno-canalicular permeability from 10^{-21} to 10^{-19} m^2 and vascular bulk modulus K_v from 12 to 16 GPa.

Wang *et al.*[30] showed their results in terms of a dimensionless pressure, defined as $P = 3p/\sigma B$, being B the Skempton coefficient. In that simulation, $tr\sigma = 4$ MPa and $B = 0.53$, so $P = 1.415p$. Also, the transcortical pressure difference (Δp) was defined as the average dimensionless pressure difference between the two external surfaces of the bone specimen. Dimensionless pressure and transcortical pressure difference are calculated in this work in order to compare the results with those of Wang *et al.*[30]

Simulation of a Whole Bone

Next, we simulate the experiments performed by Srinivasan *et al.*[24] in order to compare the influence of using a simple or dual porosity model in the fluid flow of a whole bone. For this objective, a finite element mesh of the cortical bone of a rat tibia was developed. The values of the properties of the rat tibia used in the simulation are detailed in Table 2. Due to the aligned distribution of the Haversian canals according to the longitudinal axis of the bone, vascular permeability has been modeled as transversely isotropic. To simulate the fluid boundary conditions at the periosteal and endosteal surfaces we used the same method as in Steck *et al.*,[26] creating a thin layer of elements to simulate each surface. These layers had approximately 1/4 to 1/3 of the characteristic element thickness and have a very low stiffness in order to not affect the mechanical behavior of the model. Experimental studies reported that periosteal surface was relatively impermeable to fluid flow,[18] and endosteal surface was relatively permeable.[8,17] According to these criteria, permeability in the periosteum was established

TABLE 1. Parameter values of the dual porosity model.

d_c (μm)	ϕ_1	ϕ_2	k_1 (m^2)	k_2 (m^2)	γ (m^2/Ns)
0	0	0.05	0	1.7×10^{-20}	0
40	0.03	0.05	3×10^{-13}	1.7×10^{-20}	1.7×10^{-9}
60	0.07	0.05	6.36×10^{-13}	1.7×10^{-20}	2.7×10^{-9}

TABLE 2. Parameter values of the rat tibia dual porosity model.

Longitudinal Young Modulus	$E_l = 17$ GPa
Transverse Young Modulus	$E_t = 13$ GPa
Poisson's ratios	$v_t = 0.38$ $v_{lt} = 0.41$
Vascular porosity	$\phi_1 = 0.04$
Lacuno-canalicular porosity	$\phi_2 = 0.05$
Longitudinal vascular permeability	$k_{1l} = 10^{-12}$ m^2
Transverse vascular permeability	$k_{1t} = 10^{-13}$ m^2
Lacuno-canalicular permeability	$k_2 = 10^{-20}$ m^2
Bone matrix bulk modulus	$K_s = 16000$ MPa
Interstitial fluid bulk modulus	$K_f = 2300$ MPa
Vascular bulk modulus	$K_v = 15000$ MPa
Leakage parameter	$\gamma = 1.7 \times 10^{-10}$ m^2/Ns

as $k_1 = 10^{-15}$ m^2 and $k_1 = 10^{-22}$ m^2 and in the endosteum as $k_1 = 2 \times 10^{-12}$ m^2 and $k_2 = 2 \times 10^{-19}$ m^2. The rest of the parameters were equal in both surfaces to those of cortical bone (Table 2). The resulting model was composed of 23691 nodes and 39873 elements, divided into 24272 tetrahedron elements for cortical bone and 15601 wedge elements for the periosteum and endosteum.

The tibia was fixed proximally at the tuberosity and loaded distally, being subjected to medial-lateral cantilever bending (Fig. 2a). The applied load magnitude was 0.8 N. Longitudinal strain was compared with the results of the experiments, and PLC pore pressure and fluid flow patterns were analyzed and compared with the experimental zones of new bone formation
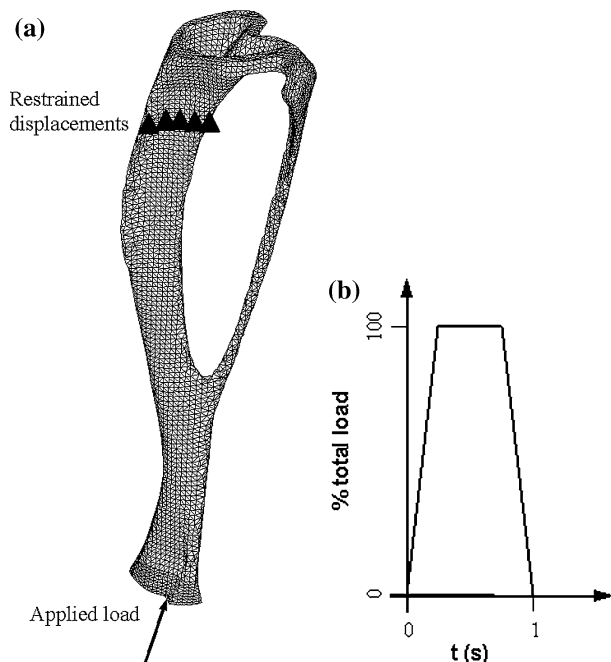

FIGURE 2. (a) Applied load and fixed zone in the model of the rat tibia. (b) Load cycle on the rat tibia.

described by Srinivasan *et al.*[24] A simple porosity analysis (only lacuno-canalicular porosity) was also performed to compare the results of single and dual porosity models.

RESULTS

Simulation of Bending of a Small Sample of Cortical Bone

After reaching the steady state, lacuno-canalicular pressure always showed the same kind of distribution pattern from the tensile side of the bone specimen (with negative pressure) to the compressive side (with positive pressure) (Fig. 3). With a loading frequency of 1.5 Hz, the pressure distribution (see Fig. 3) resulted very similar to that obtained by Starkebaum *et al.*[25] in their experimental model and by Wang *et al.*[30] in their computational one. Obviously our dual porosity model did not reproduce the cusp-like shapes around the osteonal canals, because there are no holes in our macroscopic model, but it was able to predict the transcortical distribution with enough accuracy. Lacuno-canalicular pressure in bone has a strong dependence on the diameter of the osteonal canal. Pressure value decreased considerably when the vascular porosity increased, due to the larger surface of osteonal canals and the larger number of canaliculi connected to them, allowing more bone fluid to flow from PLC to PV and viceversa.

The loading frequency has also a great influence on the maximum value of lacuno-canalicular pressure, but has almost no influence on the shape of its distribution along the bone specimen, as can be seen in Fig. 4. It is interesting to remark that these results followed a similar pattern to that included in the work of Wang *et al.*,[30] obtained by means of a microscopic model (see Fig. 1) with a pressure increase when loading frequency increased.

The value of the leakage parameter γ has a great effect on the lacuno-canalicular pressure (see Fig. 5). When γ increased, more fluid could flow from PLC to PV and then pressure in PLC decreased quickly. If γ decreased, pressure in PLC increased until a maximum value, which corresponds to the absence of vascular porosity. Lacuno-canalicular permeability k_2 also strongly influences on the fluid movement as can be seen in Fig. 6, where it becomes clear that the higher the difficulty of the fluid to flow along canaliculi (lower permeability), the higher pore fluid pressure we get. In the same sense, vascular permeability (k_1) has a great influence on the PV pressure but, on the contrary, it has a negligible influence on the PLC pressure.

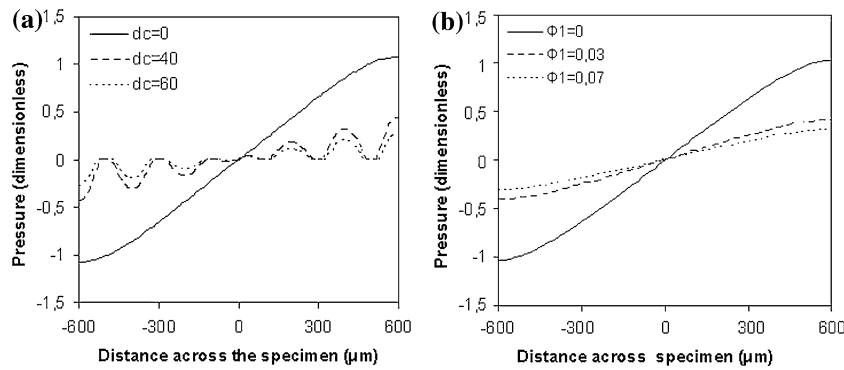Vascular compressibility K_v also influences on the PLC pressure, as can be seen in the parametric study of

FIGURE 3. Lacuno-canalicular pressure distributions across the bone specimen from inner ($y = -600$ μm) to outer ($y = 600$ μm) surfaces. Loading frequency: 1.5 Hz. (a) Model of Wang *et al.*,[30] with three values of the vascular diameter. (b) Dual porosity model, with the corresponding three values of vascular porosity.
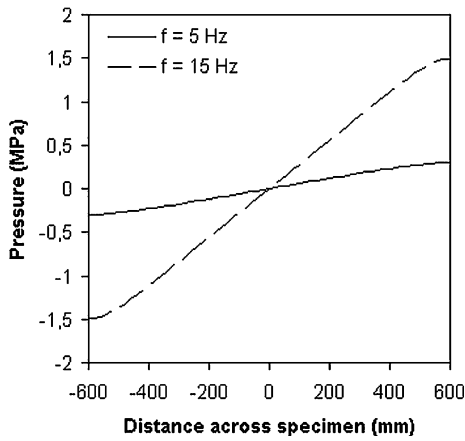

FIGURE 4. Lacuno-canalicular pressure distributions across the bone specimen from inner ($y = -600$ μm) to outer ($y = 600$ μm) surfaces, with loading frequencies of 1.5 and 15 Hz, $\phi_1 = 0.03$.

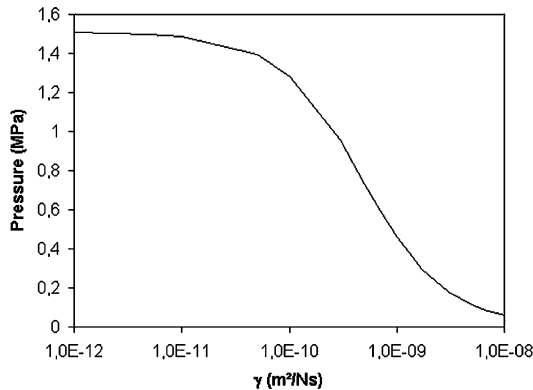**FIGURE 6.** Lacuno-canalicular pressure in the outer fiber ($y = 600$ μm) depending on the PLC permeability ($\gamma = 1.7\times 10^{-9}$ m^2/Ns, $\phi_1 = 0.03$, $f = 1.5$ Hz).

FIGURE 5. Lacuno-canalicular pressure in the outer fiber ($y = 600$ μm) depending on γ, $\phi_1 = 0.03$, $f = 1.5$ Hz.

FIGURE 7. Lacuno-canalicular pressure in the outer fiber ($y = 600$ μm) depending on the vascular compressibility K_v ($\gamma = 1.7\times10^{-9}$ m^2/Ns, $\phi_1 = 0.03$, $f = 1.5$ Hz).

this parameter (Fig. 7). The reason is that in a medium less compressible (higher K_v), the volumetric change of the medium is lower, leading to a higher fluid pressure.

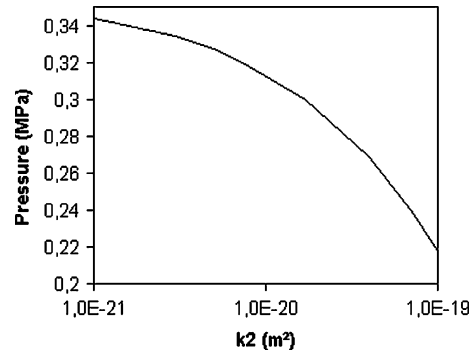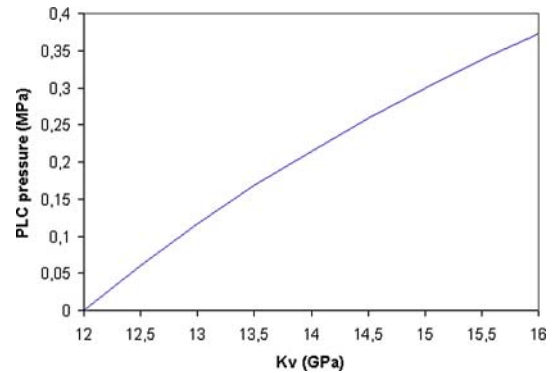Lacuno-canalicular peak pressure for the three different vascular porosities and the complete range of loading frequencies calculated, from 0.01 to 500 Hz, is represented in Fig. 8. Pressure increased with frequency until approaching asymptotically to its limiting value, $\alpha\sigma$ ($\alpha = \alpha_1 + \alpha_2$). Therefore, the lacuno-canalicular pressure at high frequencies resulted very similar, being independent on the value of vascular
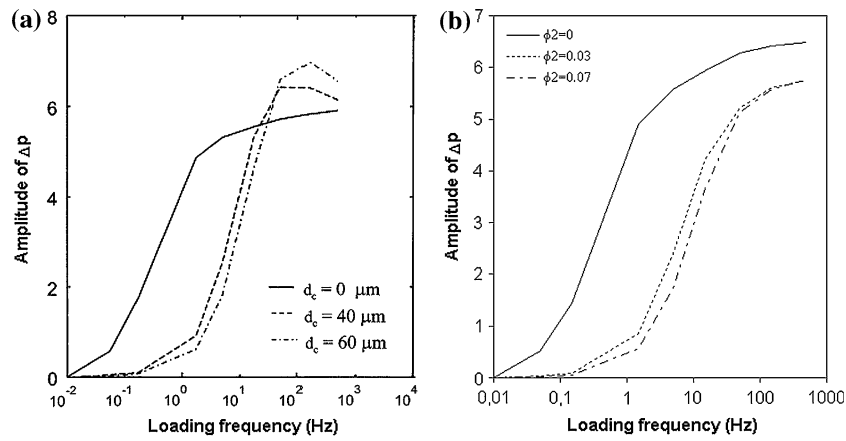
FIGURE 8. Lacuno-canalicular pressure in the outer fiber ($y = 600$ μm) depending on the frequency and PV porosity. (a) Model of Wang *et al.*[30] (b) Dual porosity model.
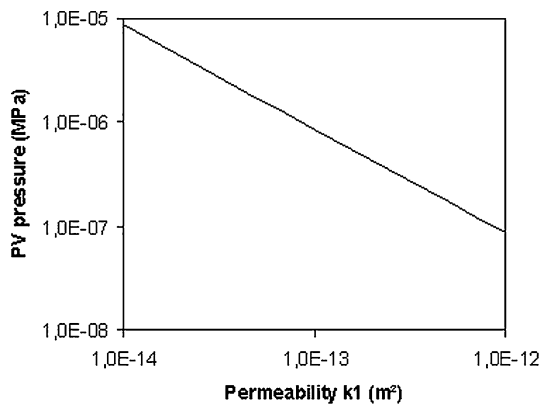

FIGURE 9. Vascular pressure in the outer fiber ($y = 600$ μm) depending on the vascular permeability k_1 ($\gamma = 1.7 \times 10^{-9}$ m²/Ns, $\phi_1 = 0.03$, $f = 1.5$ Hz).

porosity. However, for low frequencies, higher lacuno-canalicular pressures were reached for $\phi_1 = 0$.

Finally, the vascular pressure was much lower (several orders of magnitude) than the lacuno-canalicular one and depended linearly on the vascular permeability (Fig. 9).

Simulation of a Whole Bone

Resulting longitudinal strains in the rat tibia were 1500 $\mu\varepsilon$ in the periosteal surface and 1150 $\mu\varepsilon$ in the endosteal surface. Srinivasan *et al.*[24] reported case strains of 1600 and 1200 $\mu\varepsilon$, respectively. Our results showed therefore a sufficiently good agreement with the experimental ones.

PLC pressure and fluid flow in the rat tibia reached their maximum value in the mid-shaft, near the tibiofibular joint (Fig. 10). An interesting result is that fluid flow was higher in the periosteum than in the

endosteum, which is in agreement with the experiments of Srinivasan *et al.*[24] in which most of the new bone formation was concentrated on the periosteal zone.

A comparison between single and double porosity models of the rat tibia showed that the fluid flow reaches higher peak values in the single porosity model (2×10^{-5} mm/s with single porosity, 10^{-5} mm/s with double porosity, see Fig. 11). This result is in agreement with that of the small sample of cortical bone and corroborates that vascular porosity has a remarkable effect relaxing pressure, pressure gradients, and fluid
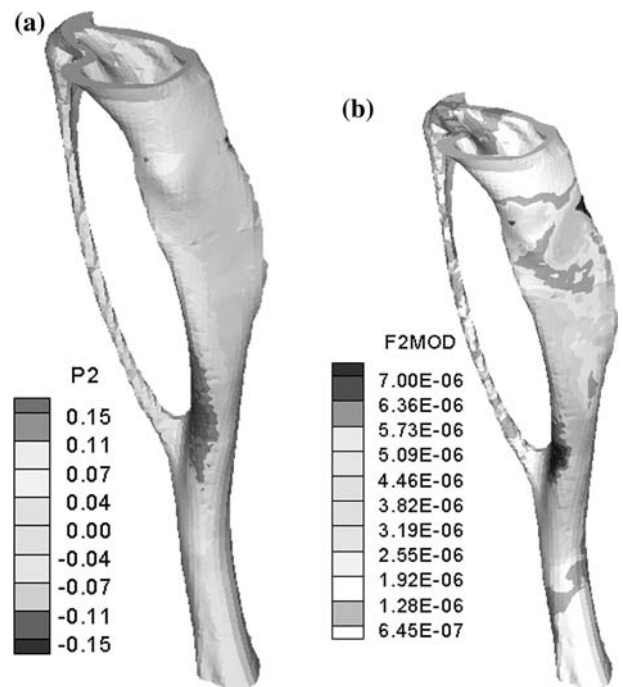

FIGURE 10. (a) PLC pressure (MPa) and (b) modulus of the PLC fluid flow (mm/s) in the rat tibia.
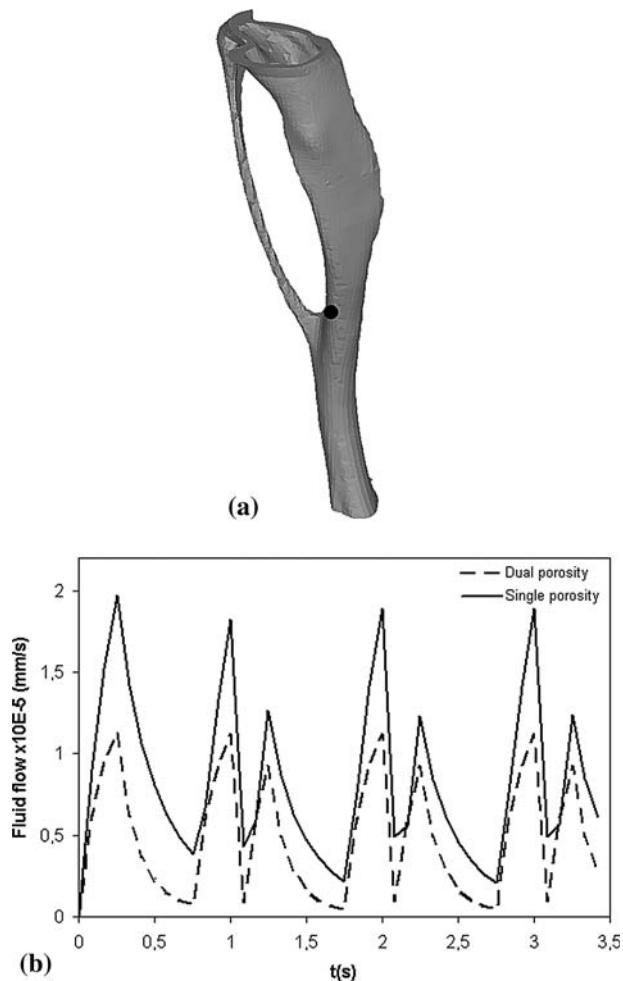
FIGURE 11. **(b) Time evolution of the lacuno-canalicular fluid flow modulus of the rat tibia at the location shown in (a).**

flow in the lacuno-canalicular system, apart from its well-known function of carrying nutrients and wastes.

When the applied load was increasing, in the beginning of the load cycle, the fluid flowed in the tibia from the compressive to the tensile side, while in the end of the cycle, when the load was decreasing, the fluid flow direction inverted. In the mid-phase of the cycle the applied load was constant, and consequently fluid flow experimented relaxation during this phase.

DISCUSSION

A finite element dual porosity model has been developed to calculate the mechanically load-induced fluid flow at different bone porous networks: PV and PLC. Treating bone as a continuum, using macroscopic poroelastic properties that characterizes the two levels of porosity and defining a leakage parameter that describes the rate of flow between them, we were able to model complex bone behaviors.

Using this model is advantageous with respect to classical poroelastic models with only one level of porosity, since we are now able to simulate a whole loaded bone and estimate very well both vascular and lacuno-canalicular pressures at least in average since this is a continuum macroscopic approach. These results can be very useful for a better understanding of the macroscopic role that fluid flow plays in mechanotransduction phenomena at lacuno-canalicular level related to the global mechanical bone environment. In fact, this model can help to understand the bone transport capacity through the fluid movement from bone vasculature to canaliculi and lacunae in bone extracellular matrix.

In order to check the potential of this dual porosity model, we studied the example shown by Starkebaum et al.,[25,30] which consisted on a sinusoidal bending load applied to a little sample of cortical bone. Our results showed the same general trend that those obtained experimentally,[25] with a pressure gradient between tensile and compressive fibers. The experiment of Starkebaum et al.[25] and the simulations of Wang et al.[30] also showed a cusp-like form gradients near the Haversian canals. Our model is not able to predict these gradients due to heterogeneous structure of cortical bone, because it is a macroscopic approach and the Haversian canals are not physically considered in the model. This aspect is one of the main limitations of our model if you are interested on estimating the fluid flow shear stress along the cells and not the averaged flows. The use of a multiscale formulation combining a micro–macroscopic approach in which the microscopic effects control the macroscopic behavior could be an important tool to surpass this limitation. Nevertheless, the model here presented is able to predict the global distribution pattern of the lacuno-canalicular pressure and flow.

Another microscopic effect that we have not considered in the model is the difference between canalicular and lacunar porosities.[14] In fact, Gururaja et al.[14] showed that there is a gradient of fluid pressures in the canaliculi that leads to flow into and out of the lacuna due to the heterogeneity of the deformation around a lacuna. Again, this effect could be taken into account by means of multi-scale models that incorporate the different levels of bone poroelasticity.

We have also studied the influence of the mechanical loading frequency, concluding that higher load frequencies increase considerably the fluid flow at the canalicular level. This effect has been also observed experimentally.[9,27,32] Lacuno-canalicular pressure decreases when vascular porosity is modeled due to the pressure relaxation induced by fluid flowing from PLC to PV. Frequency analysis involves a large range from 0.01 to 500 Hz. Since this dual-porosity model neglects

inertial effects, the approximation at high frequencies could not be sufficiently accurate, although it is enough to show the main trend of the frequency influence and compare our results with those presented by Wang *et al.*[30] that used the same approximation.

From our results, we can observe that PLC and PV pressures differ in several orders of magnitude. This fact has a clear meaning, because while fluid in PLC has to transport nutrients to the osteocytes network through the very thin canaliculi, PV fluid never surpass the capillarity pressure (about 0.05 atm[33]) to allow a normal blood supply into the bone.

Strains usually applied to bone (0.04 to 0.3%) are much smaller than those needed to cause bone signalling in deformed cell cultures (1–10%),[13,22,29] so it is widely believed that there must be a mechanism that amplifies the external stimulus at cellular level.[9] This mechanism is reflected indirectly by fluid flow at PLC, a mechanical stimulus that can be sensed by osteocytes. Zhang *et al.*[32] estimated that the maximum pressure at an osteon is about 0.27 MPa and is reached at the cement line. In our simulation, the maximum lacuno-canalicular pressure is in the range of 0.2–0.3 MPa for dual porosity simulations and a physiological frequency of 1.5 Hz.

The parameters from our model that mainly regulate this stimulus amplification are γ (the leakage parameter), k_2 (the lacuno-canalicular permeability) and vascular compressibility K_v. If γ is too small, fluid exchange between PV and PLC is not enough to accomplish its function of transporting nutrients to osteocytes and evacuate waste from them, but if it is too high, the pore pressure decreases in the canaliculi and the amplification mechanism disappears. If the permeability of PLC increases, fluid can flow more freely along the canaliculi, and the pore pressure in PLC decreases. Our results show that, when the model takes into account the PV, the pressure decreasing in PLC is remarkable. We think that this suggests that the role of the PV is not only to provide blood and nutrients supply, but also to contribute to the regulation of the PLC pressure.

An accurate estimation of the leakage parameter would require a detailed study of the microstructural interaction between Haversian canals and canaliculi. Parameters such as the spacing between Haversian canals or the density and permeability of the canaliculi attached to them have a crucial influence on the value of γ. The leakage parameter also probably depends on the loading frequency. The value of γ cannot be determined with a macroscopic model, being necessary to achieve this objective the use of a multiscale model that allows evaluating this parameter at the microscopic level to be next used at the macroscopic one.

Since permeability values in bone are subjected to considerable uncertainty, typical values have been taken from literature in this model.[8] Nevertheless, a sensitivity analysis has been performed in order to know the influence of these values. In fact, permeability of PV has practically no influence on the stimulus that osteocytes sense. However, permeability of the PLC is a characteristic parameter of the fluid flow in canaliculi: higher PLC permeability leads to lower PLC pressure as it is clearly shown in Fig. 6.

Another key point is the estimation of the vascular compressibility. The value of the K_v used in this work has been estimated through a microscopic finite element computational model. In order to know the influence of this property, a sensitivity analysis has been performed and it has revealed a high dependency of the lacuno-canalicular pressure on the vascular compressibility K_v (see Fig. 7).

The three dimensional analysis of the rat tibia showed a good agreement with the experiments. Lacuno-canalicular pressure and fluid flow resulted higher in the zones where the new bone formation was reported. There was also a significant difference in peak values between single and double porosity model. These results suggest that the employment of the dual porosity model may allow to estimate the variables with decisive impact on bone behavior and incorporate them in future bone remodeling models. Therefore, this simulation demonstrates the great potential of this dual porosity approach to study the complexity of a whole loaded bone in an easy way via a macroscopic model.

Although we think this macroscopic approach is appropriate for the estimation of the averaged fluid flows and pressures at both vascular and canalicular porosities, a better and more complex multiscale formulation could be used. And so, a combination of macroscopic with microscopic approach could model the different levels of porosity of cortical bone, enhancing the evaluation of fluid flows and pressures at these porosities. This sophisticated model, however, would imply a high computational cost that would be necessary to evaluate. Therefore, depending on the objective to analyse, a macroscopic model or a micro–macro approach can be appropriate.

In our case, we are interested on the development of a computational model able to simulate bone functional capacity to adapt its properties to mechanical and metabolic environment changes. When a whole loaded bone is analyzed to simulate this adaptative property, a phenomenological stimulus is normally required to control this process. Currently, research work has described that fluid flow induced by mechanical load in the osteocytic network is the main factor that regulates mechanosensory bone system by

different ways: nutrition and removal of waste substances, shear stresses or streaming potentials.[9] Therefore, in order to achieve more biophysically-based stimuli, this phenomenological stimulus has to be related to this bone fluid flow. The keypoint is to know if the mechanobiological bone response due to osteoblasts and osteoclasts is regulated by osteocytes individually, or if it is controlled by a set of osteocytes interconnected. In the first situation, probably is necessary to estimate the fluid flow at osteocyte level, but in the second one is probably enough to determine the averaged fluid flow. Therefore, and as a first hypothesis, we consider that averaged fluid flow at lacuno-canalicular level can be sufficient to estimate mechanical stimuli valid for bone remodeling, although more complex multiscale approaches can be used to improve fluid flow estimation in a loaded bone.

APPENDIX A: DUAL POROSITY MODEL

For saturated porous media (like cortical bone tissue), the equilibrium equations can be written as

$$\frac{\partial \tau_{ij}}{\partial x_j} + F_i = 0 \qquad (4)$$

where F_i is the body force per unit volume and τ_{ij} is the total stress that can be expressed as

$$\tau_{ij} = \sigma_{ij} - \alpha_1 p_1 \delta_{ij} - \alpha_2 p_2 \delta_{ij} \qquad (5)$$

being σ_{ij} the effective stress, p_1 and p_2 the pore fluid pressures in the two levels of porosity (here PV and PLC), α_1 and α_2 the effective stress coefficients and δ_{ij} the Kronecker's delta. For an elastic and isotropic bone matrix, the effective stress can be written as

$$\sigma_{ij} = 2G\varepsilon_{ij} + \lambda\varepsilon_{kk}\delta_{ij} \qquad (6)$$

with ε_{ij} the global strain tensor and λ and G the so called Lame's constants, that are expressed in terms of the Young's modulus E and the Poisson's ratio v as $\lambda = Ev/(1 + v)(1 - 2v)$ and $G = E/2(1 + v)$.

The governing equation for the solid phase is obtained combining Eqs. (4), (5) and (6) getting:

$$2G\frac{\partial \varepsilon_{ij}}{\partial x_j} + \lambda\frac{\partial \varepsilon_{jj}}{\partial x_i} - \alpha_1\frac{\partial p_1}{\partial x_i} - \alpha_2\frac{\partial p_2}{\partial x_i} + F_i = 0 \qquad (7)$$

For small deformations, strains are related to displacements by the well-known Cauchy strain tensor

$$\varepsilon_{ij} = \frac{1}{2}\left(\frac{\partial u_i}{\partial x_j} + \frac{\partial u_j}{\partial x_i}\right) \qquad (8)$$

with $\boldsymbol{u}$ the displacement vector. Substituting Eq. (8) into (7), the governing equation of the solid phase can we written as a function of displacements as

$$G\frac{\partial^2 u_i}{\partial x_j \partial x_j} + (\lambda + G)\frac{\partial^2 u_j}{\partial x_i \partial x_j} - \alpha_1\frac{\partial p_1}{\partial x_i} - \alpha_2\frac{\partial p_2}{\partial x_i} + F_i = 0 \qquad (9)$$

The definition of the effective stress parameters α_1 and α_2 can be determined in terms of physically measurable parameters. Following the procedure of Khalili and Valliappan,[15] a representative planar volume of cortical bone is subjected to external principal stresses σ_{ii} and to internal vascular pressure p_1 and lacuno-canalicular pressure p_2. These stresses can be decomposed in four components, as it is shown in Fig. 12: (I) equal PV, PLC and external hydrostatic pressure p_1; (II) zero PV pressure and equal PLC and external hydrostatic pressure $(p_2 - p_1)$; (III) external hydrostatic pressure $(\overline{\sigma} - p_2)$, being $\overline{\sigma} = \sigma_{ii}/3$; and (IV) external deviator stress $\widetilde{\sigma}_{ij} = \sigma_{ij} - \overline{\sigma}\delta_{ij}$. The total volumetric strain of this representative bone volume may be calculated, according to Nur and Byerlee,[21] as

$$\varepsilon_{ii} = \varepsilon_{ii}^{\mathrm{I}} + \varepsilon_{ii}^{\mathrm{II}} + \varepsilon_{ii}^{\mathrm{III}} + \varepsilon_{ii}^{\mathrm{IV}} \qquad (10)$$

being

$$\varepsilon_{ii}^{\mathrm{I}} = \frac{p_1}{K_{\mathrm{s}}} \qquad (11a)$$

$$\varepsilon_{ii}^{\mathrm{II}} = \frac{p_2 - p_1}{K_{\mathrm{v}}} \qquad (11b)$$

$$\varepsilon_{ii}^{\mathrm{III}} = \frac{\overline{\sigma} - p_2}{K} \qquad (11c)$$

$$\varepsilon_{ii}^{\mathrm{IV}} = 0 \qquad (11d)$$

where K_{s}, K_{v} and K are the drained bulk modulus of the bone matrix, the vascular porosity and the cortical bone, respectively. Introducing Eq. (11) into (10) and rearranging, the volumetric strain results

$$\varepsilon_{ii} = \frac{\overline{\sigma}}{K} - \left(\frac{1}{K_{\mathrm{v}}} - \frac{1}{K_{\mathrm{s}}}\right)p_1 - \left(\frac{1}{K} - \frac{1}{K_{\mathrm{v}}}\right)p_2 \qquad (12)$$

Applying now the definition of effective stress, it can also be written as

$$\varepsilon_{ii} = \frac{1}{K}(\overline{\sigma} - \alpha_1 p_1 - \alpha_2 p_2) \qquad (13)$$

Comparing Eqs. (12) and (13) yields

$$\alpha_1 = \frac{K}{K_{\mathrm{v}}} - \frac{K}{K_{\mathrm{s}}} \qquad \alpha_2 = 1 - \frac{K}{K_{\mathrm{v}}} \qquad (14)$$

Note that when the lacuno-canalicular porosity is reduced to zero (i.e. $K_{\mathrm{v}} = K$), the stress effective coefficients are those used in single porosity models ($\alpha_1 = 1 - K/K_{\mathrm{s}}$, $\alpha_2 = 0$).
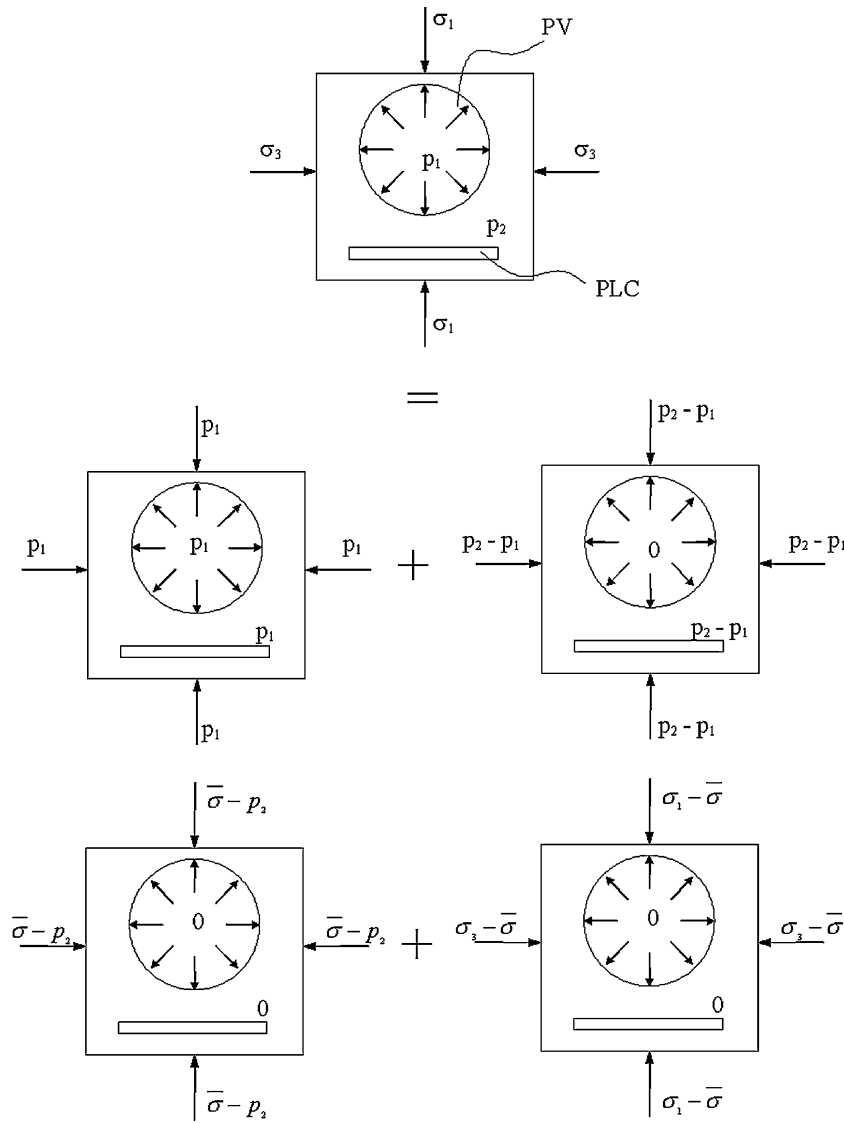
FIGURE 12. Stress decomposition of a representative bone element. The component normal to the plane, σ_2, is not shown for simplicity.

The governing equations for fluid flow in PV and PLC can be obtained from the mass conservation equations for the fluid. Darcy's law has been considered here as the constitutive equation, that is,

$$v_{\alpha i} = -\frac{k_\alpha}{\mu}\frac{\partial p_\alpha}{\partial x_i} \quad \alpha = 1, 2 \qquad (15)$$

being k the permeability of the pore network and μ the viscosity of the fluid. Subindex α takes the value 1 for the PV and 2 for the PLC, and $v_{\alpha i}$ represents the relative fluid velocity in each network with respect to the bone matrix, that can be expressed in terms of the porosity ϕ_α, the absolute velocity $v_{\alpha i f}$ and the velocity of the bone matrix v_{is} as

$$v_{\alpha i} = \phi_\alpha(v_{\alpha i f} - v_{is}) \quad \alpha = 1, 2 \qquad (16)$$

Mass conservation of the fluid in the PV and PLC networks can be written as

$$-\frac{\partial}{\partial x_i}(\rho_f \phi_\alpha v_{\alpha i f}) = \frac{\partial}{\partial t}(\phi_\alpha \rho_f) - (-1)^\alpha \Gamma \quad \alpha = 1, 2 \quad (17)$$

where Γ corresponds to the leakage term that represents the rate of flow between canaliculi and Haversian canals. Substitution of Eq. (16) into (17) yields

$$-\frac{\partial}{\partial x_i}(\rho_f v_{\alpha i}) - \frac{\partial}{\partial x_i}(\rho_f \phi_\alpha v_{is}) = \frac{\partial}{\partial t}(\phi_\alpha \rho_f) - (-1)^\alpha \Gamma \quad \alpha = 1, 2$$

$$(18)$$

which, introducing the Lagrangian material derivative relative to the solid ($d_s()/dt = \partial()/\partial t + v_{is}\partial()/\partial x_i$) can be rearranged as

$$-\frac{\partial}{\partial x_i}(\rho_{\mathrm{f}} v_{\alpha i}) = \phi_\alpha \frac{d_{\mathrm{s}}\rho_{\mathrm{f}}}{dt} + \rho_{\mathrm{f}} \frac{d_{\mathrm{s}}\phi_\alpha}{dt}$$
$$+ \rho_{\mathrm{f}}\phi_\alpha \frac{\partial v_{is}}{\partial x_i} - (-1)^\alpha \Gamma \quad \alpha = 1, 2 \quad (19)$$

According to the definition of compressibility one can write for the fluid

$$\frac{1}{\rho_{\mathrm{f}}}\frac{d_{\mathrm{s}}\rho_{\mathrm{f}}}{dt} = \frac{1}{K_{\mathrm{f}}}\frac{d_{\mathrm{s}}p_\alpha}{dt} \quad \alpha = 1, 2 \quad (20)$$

Substituting Eqs. (15) and (20) into (19) divided by ρ_{f} it results in

$$\frac{1}{\rho_{\mathrm{f}}}\frac{\partial}{\partial x_i}\left(\rho_{\mathrm{f}}\frac{k_\alpha}{\mu}\right)\frac{\partial p_\alpha}{\partial x_i} = \frac{\phi_\alpha}{K_{\mathrm{f}}}\frac{d_{\mathrm{s}}p_\alpha}{dt} + \frac{d_{\mathrm{s}}\phi_\alpha}{dt}$$
$$+ \phi_\alpha \frac{\partial v_{is}}{\partial x_i} - (-1)^\alpha \frac{\Gamma}{\rho_{\mathrm{f}}} \quad \alpha = 1, 2$$
$$(21)$$

Equations (9) and (21) conform the governing equations system for cortical bone. However, in order to completely solve these equations another relationship is needed to establish the term $d_{\mathrm{s}}\phi_\alpha/dt$. This relationship can be derived from the definition of porosities

$$\phi_\alpha = \frac{V_\alpha}{V} \quad \alpha = 1, 2 \quad (22)$$

where V is a representative volume of cortical bone, and V_1 and V_2 are the volumes of PV and PLC in that representative volume. Differentiation of Eq. (22) yields

$$d\phi_\alpha = \frac{1}{V}(dV_\alpha - \phi_\alpha dV) \quad \alpha = 1, 2 \quad (23)$$

The last term in Eq. (23) is actually related to the volumetric strain of the matrix

$$\frac{dV}{V} = tr\varepsilon = \frac{\partial u_{is}}{\partial x_i} \quad (24)$$

and, for the first terms in the right-hand side of Eq. (23), which correspond to the variation in fluid content of each porosity ζ_α, Khalili and Valliappan[15] showed that they can be expressed as

$$\frac{dV_1}{V} = \zeta_1 = \alpha_1 \frac{\partial u_{is}}{\partial x_i} + \frac{\alpha_1 - \phi_1}{K_{\mathrm{s}}}dp_1 + \frac{\chi}{K}d(p_1 - p_2)$$
$$(25a)$$

$$\frac{dV_2}{V} = \zeta_2 = \alpha_2 \frac{\partial u_{is}}{\partial x_i} + \frac{\alpha_2 - \phi_2}{K_{\mathrm{s}}}dp_2 + \frac{\chi}{K}d(p_2 - p_1)$$
$$(25b)$$

$$\chi = \alpha_1\alpha_2 - \phi_1\phi_2\frac{\alpha_1 + \alpha_2}{\phi_1 + \phi_2} \quad (25c)$$

Applying (23) in (21) and considering that, in general, $v_{is}\partial()/\partial x_i \ll \partial()/\partial t$ and then $d_{\mathrm{s}}()/dt \approx \partial()/\partial t$, it results into

$$\frac{k_1}{\mu}\frac{\partial^2 p_1}{\partial x_i \partial x_i} = \left(\frac{\phi_1}{K_{\mathrm{f}}} + \frac{\alpha_1 - \phi_1}{K_{\mathrm{s}}} + \frac{\chi}{K}\right)\frac{\partial p_1}{\partial t}$$
$$-\frac{\chi}{K}\frac{\partial p_2}{\partial t} + \alpha_1\frac{\partial v_{is}}{\partial x_i} - \frac{\Gamma}{\rho_{\mathrm{f}}}$$
$$(26a)$$

$$\frac{k_2}{\mu}\frac{\partial^2 p_2}{\partial x_i \partial x_i} = \left(\frac{\phi_2}{K_{\mathrm{f}}} + \frac{\alpha_2 - \phi_2}{K_{\mathrm{s}}} + \frac{\chi}{K}\right)\frac{\partial p_2}{\partial t}$$
$$-\frac{\chi}{K}\frac{\partial p_1}{\partial t} + \alpha_2\frac{\partial v_{is}}{\partial x_i} + \frac{\Gamma}{\rho_{\mathrm{f}}}$$
$$(26b)$$

and recovering Eq. (9) the complete set of governing equations for the bone cortical tissue becomes

$$G\frac{\partial^2 u_i}{\partial x_j \partial x_j} + (\lambda + G)\frac{\partial^2 u_j}{\partial x_i \partial x_j} - \alpha_1\frac{\partial p_1}{\partial x_i} - \alpha_2\frac{\partial p_2}{\partial x_i} + F_i = 0$$
$$(27a)$$

$$\frac{k_1}{\mu}\frac{\partial^2 p_1}{\partial x_i \partial x_i} = a_{11}\frac{\partial p_1}{\partial t} + a_{12}\frac{\partial p_2}{\partial t} + \alpha_1\frac{\partial^2 u_i}{\partial t \partial x_i} - \frac{\Gamma}{\rho_{\mathrm{f}}} \quad (27b)$$

$$\frac{k_2}{\mu}\frac{\partial^2 p_2}{\partial x_i \partial x_i} = a_{21}\frac{\partial p_1}{\partial t} + a_{22}\frac{\partial p_2}{\partial t} + \alpha_2\frac{\partial^2 u_i}{\partial t \partial x_i} + \frac{\Gamma}{\rho_{\mathrm{f}}} \quad (27c)$$

$$\frac{\Gamma}{\rho_{\mathrm{f}}} = \gamma(p_1 - p_2) \quad (27d)$$

where γ is the so-called leakage parameter, which modulates the regulating role that bone lining cells perform on bone surfaces controlling the flux of fluid between compartments and the interstitial fluid pressure.[16] The rest of the parameters are defined as

$$a_{11} = \phi_1/K_{\mathrm{f}} + (\alpha_1 - \phi_1)/K_{\mathrm{s}} + \chi/K$$
$$a_{12} = a_{21} = -\chi/K$$
$$a_{22} = \phi_2/K_{\mathrm{f}} + (\alpha_2 - \phi_2)/K_{\mathrm{s}} + \chi/K \quad (28)$$
$$\alpha_1 = K/K_{\mathrm{v}} - K/K_{\mathrm{s}}$$
$$\alpha_2 = 1 - K/K_{\mathrm{v}}$$

REFERENCES

[1]Aiffantis, E. C. Introducing a multi-porous media. *Develop. Mech*. 8:209–211, 1977.

[2]Aiffantis, E. C. On the response of fissured rocks. *Develop. Mech*. 10:249–253, 1979.

[3]Anderson, E. J., S. Kaliyamoorthy, J. I. D. Alexander, and M. L. Knothe Tate. Nano-microscale models of periosteocytic flow show differences in stresses imparted to cell body processes. *Ann. Biomed. Eng*. 33(1):52–62, 2005.

[4]Bacabac, R. G., T. H. Smit, M. G. Mullender, J. J. W. A. Van Loon, and J. Klein-Nulend. Initial stress-kick is required for fluid shear stress-induced rate dependent activation bone cells. *Ann. Biomed. Eng*. 33(1):104–110, 2005.

[5]Beno, T., Y. Yoon, S. C. Cowin, and S. P. Fritton. Estimation of bone permeability using accurate microstructural measurements. *J. Biomech*. 39:2378–2387, 2006.

[6]Biot, M. A. General theory of three-dimensional consolidation. *J. Appl. Phys*. 12:155–164, 1941.

[7]Burger, E. H., J. Klein-Nulend, and T. H. Smit. Strain-derived canalicular fluid flow regulates osteoclast activity in a remodelling osteon – a proposal. *J. Biomech*. 36:1453–1459, 2003.

[8]Cowin, S. C. Bone poroelasticity. *J. Biomech*. 32:217–238, 1999.

[9]Cowin, S. C. Mechanosensation and fluid transport in living bone. *J. Muskuloske Neuron. Interact*. 2(3):256–260, 2002.

[10]Duguid, J. O. Flow in fractured porous media. PhD Thesis. New Jersey: Princeton University, 1973.

[11]Duguid, J. O., and J. Abel. Finite element Galerkin method for flow in fractured porous media. In: Finite Element Methods in Flow Problems, edited by Gallagher et al. Huntsville: UAH Press, 1974, pp. 559–615.

[12]Duguid, J. O., and P. C. Y. Lee. Flow in fractured porous media. *Water Resour. Res*. 13:558–566, 1977.

[13]Fritton, S. P., K. J. McLeod, and C. T. Rubin. Quantifying the strain history of bone: spatial uniformity and self-similarity of low-magnitude strains. *J. Biomech*. 33:317–325, 2000.

[14]Gururaja, S., H. J. Kim, C. C. Swan, R. A. Brand, and R. S. Lakes. Modeling deformation-induced fluid flow in cortical bone's canalicular-lacunar system. *Ann. Biomed. Eng*. 33(1):7–25, 2005.

[15]Khalili-Naghadesh, N., and S. Valliappan. Unified theory of flow and deformation in double porous media. *Eur. J. Mech. A/Solid* 15:321–336, 1996.

[16]Knothe Tate, M. L. Interstitial fluid flow. In: Bone Mechanics Handbook, edited by S. C. Cowin. Boca Raton: CRC Press, 1989.

[17]Knothe Tate, M. L., P. Niederer, and U. Knothe. In vivo tracer transport through the lacunocanalicular system of rat bone in an environment devoid of mechanical loading. *Bone* 22(2):107–117, 1998.

[18]Li, G. P., J. T. Bronk, K. N. An, and P. J. Kelly. Permeability of cortical bone of canine tibiae. *Microvasc. Res*. 34:302–310, 1987.

[19]Mak, A. F. T., D. T. Huang, J. D. Zhang, and P. Tong. Deformation-induced hierarchical flows and drag forces in bone canaliculi and matrix microporosity. *J. Biomech*. 30:11–18, 1997.

[20]Hibbit, Karlsson and Sorensen, Inc. Abaqus user's Manual, v. 6.3. HKS inc. Pawtucket, RI, USA, 2002.

[21]Nur, A., and J. D. Byerlee. An exact effective stress law for elastic deformation of rocks with fluids. *J. Geophys. Res*. 76:6414–6419, 1971.

[22]Rubin, C. T., and L. E. Lanyon. Regulation of bone formation by applied dynamic loads. *J. Bone Join Sur*. 66A:397–415, 1984.

[23]Smit, T. H., E. H. Burger, and J. M. Huyghe. A case for strain-induced fluid flow as regulator of BMU-coupling and osteonal alignment. *J. Bone Miner. Res*. 17(11):2021–2029, 2002.

[24]Srinivasan, S., S. C. Agans, K. A. King, N. Y. Moy, S. L. Poliachik, and T. S. Gross. Enabling bone formation in the aged skeleton via rest-inserted mechanical loading. *Bone* 33:946–955, 2003.

[25]Starkebaum, W., S. R. Pollack, and E. Korostoff. Microelectrode studies of stress-generated potential in four-point bending of bone. *J. Biomed. Mater. Res*. 13:729–751, 1979.

[26]Steck, R., P. Niederer, and M. L. Knothe Tate. A Finite Element analisis for the prediction of load-induced fluid flow and mechanochemical transduction in bone. *J. Theor. Biol*. 220:249–259, 2003.

[27]Swan, C. C., R. S. Lakes, R. A. Brand, and K. J. Stewart. Micromechanically based poroelastic modeling of fluid flow in haversian bone. *J. Biomech. Eng*. 125:25–37, 2003.

[28]Valliappan, S., and N. Khalili-Naghadesh. Flow through fissured porous media with deformable matrix. *Int. J. Numerical Methods Eng*. 29:1079–1094, 1990.

[29]You, J., C. E. Yellowley, H. J. Donahue, Y. Zhang, Q. Chen, and C. R. Jacobs. Substrate deformation levels associated with routine physical activity are less stimulatory to bones cells relative to loading-induced oscillatory fluid flow. *J Biomech Eng* 122:387–393, 2000.

[30]Wang, L., S. P. Fritton, S. C. Cowin, and S. Weinbaum. Fluid pressure relaxation depends upon osteon microstructure: modelling an oscillatory bending experiment. *J. Biomech*. 32:663–672, 1999.

[31]Wolff, J. Das gesetz der transformation der knochen. Berlin: Hirschwald, 1892.

[32]Zhang, D., S. Weinbaum, and S. C. Cowin. On the calculation of bone pore water pressure due to mechanical loading. *Int. J. Solids Structures* 35:4981–4997, 1998.

[33]Zhang, D., S. Weinbaum, and S. C. Cowin. Estimates of the peak pressures in bone pore water. *J. Biomech. Eng*. 120:697–703, 1998.

[34]Zienkiewicz, O. C., and T. Shiomi. Dynamic behaviour of porous media; the generalized Biot formulation and its numerical solution. *Int. J. Num. Anal. Meth. Geomech*. 8(1):71–96, 1984.